

Electronic and optical properties of 3N-doped graphdiyne/MoS_2 heterostructures tuned by biaxial strain and external electric field

Dong Wei(魏东), Yi Li(李依), Zhen Feng(冯振), Gaofu Guo(郭高甫), Yaqiang Ma(马亚强), Heng Yu(余恒), Qingqing Luo(骆晴晴), Yanan Tang(唐亚楠), and Xianqi Dai(戴宪起)

Citation: Chin. Phys. B, 2021, 30 (**11**): 117103. DOI: 10.1088/1674-1056/ac1927
Journal homepage: http://cpb.iphy.ac.cn; http://iopscience.iop.org/cpb

What follows is a list of articles you may be interested in

First-principles investigation of the valley and electrical properties of carbon-doped α-graphyne-like BN sheet

Bo Chen(陈波), Xiang-Qian Li(李向前), Lin Xue(薛林), Yan Han(韩燕), Zhi Yang(杨致), and Long-Long Zhang(张龙龙)

Chin. Phys. B, 2021, 30 (**5**): 057101. DOI: 10.1088/1674-1056/abddac

Interfacial properties of g-C_3N_4/TiO_2 heterostructures studied by DFT calculations

Chen-Shan Peng(彭春山), Yong-Dong Zhou(周永东), Sui-Shuan Zhang(张虽栓), and Zong-Yan Zhao(赵宗彦)

Chin. Phys. B, 2021, 30 (**1**): 017101. DOI: 10.1088/1674-1056/abb30b

Electronic properties of size-dependent $MoTe_2$/WTe_2 heterostructure

Jing Liu(刘婧), Ya-Qiang Ma(马亚强), Ya-Wei Dai(戴雅薇), Yang Chen(陈炀), Yi Li(李依), Ya-Nan Tang(唐亚楠), Xian-Qi Dai(戴宪起)

Chin. Phys. B, 2019, 28 (**10**): 107101. DOI: 10.1088/1674-1056/ab3b53

Prediction of high-mobility two-dimensional electron gas at $KTaO_3$-based heterointerfaces

Fu-Ning Wang(王芙凝), Ji-Chao Li(李吉超), Yi Li(李宜), Xin-Miao Zhang(张鑫淼), Xue-Jin Wang(王学晋), Yu-Fei Chen(陈宇飞), Jian Liu(刘剑), Chun-Lei Wang(王春雷), Ming-Lei Zhao(赵明磊), Liang-Mo Mei(梅良模)

Chin. Phys. B, 2019, 28 (**4**): 047101. DOI: 10.1088/1674-1056/28/4/047101

A theoretical investigation of the band alignment of type-I direct band gap dilute nitride phosphide alloy of $GaN_xAs_yP_{1-x-y}$/GaP quantum wells on GaP substrates

Ö L Ünsal, B Gönül, M Temiz

Chin. Phys. B, 2014, 23 (**7**): 077104. DOI: 10.1088/1674-1056/23/7/077104

Electronic and optical properties of 3N-doped graphdiyne/MoS_2 heterostructures tuned by biaxial strain and external electric field*

Dong Wei(魏东)[1], Yi Li(李依)[1], Zhen Feng(冯振)[1,2], Gaofu Guo(郭高甫)[1], Yaqiang Ma(马亚强)[1], Heng Yu(余恒)[1], Qingqing Luo(骆晴晴)[1], Yanan Tang(唐亚楠)[3], and Xianqi Dai(戴宪起)[1,†]

[1] *School of Physics, Henan Normal University, Xinxiang* 453007, *China*

[2] *School of Materials Science and Engineering, Henan Engineering Research Center for Modification Technology of Metal Materials, Henan Institute of Technology, Xinxiang* 453000, *China*

[3] *School of Physics and Electronic Engineering, Zhengzhou Normal University, Zhengzhou* 450044, *China*

(Received 9 May 2021; revised manuscript received 4 July 2021; accepted manuscript online 30 July 2021)

The construction of van der Waals (vdW) heterostructures by stacking different two-dimensional layered materials have been recognised as an effective strategy to obtain the desired properties. The 3N-doped graphdiyne (N-GY) has been successfully synthesized in the laboratory. It could be assembled into a supercapacitor and can be used for tensile energy storage. However, the flat band and wide forbidden bands could hinder its application of N-GY layer in optoelectronic and nanoelectronic devices. In order to extend the application of N-GY layer in electronic devices, MoS_2 was selected to construct an N-GY/MoS_2 heterostructure due to its good electronic and optical properties. The N-GY/MoS_2 heterostructure has an optical absorption range from the visible to ultraviolet with a absorption coefficient of 10^5 cm^{-1}. The N-GY/MoS_2 heterostructure exhibits a type-II band alignment allows the electron–hole to be located on N-GY and MoS_2 respectively, which can further reduce the electron–hole complexation to increase exciton lifetime. The power conversion efficiency of N-GY/MoS_2 heterostructure is up to 17.77%, indicating it is a promising candidate material for solar cells. In addition, the external electric field and biaxial strain could effectively tune the electronic structure. Our results provide a theoretical support for the design and application of N-GY/MoS_2 vdW heterostructures in semiconductor sensors and photovoltaic devices.

Keywords: two-dimensional layer materials, heterostructures, electronic structure, power conversion efficiency

PACS: 71.15.Mb, 73.22.–f, 88.40.H– **DOI:** 10.1088/1674-1056/ac1927

1. Introduction

Since graphene was successfully mechanical exfoliated in 2004,[1] an increasing number of two-dimensional layered materials (2DLMs) have been synthesized experimentally and used in research.[2–6] As the research progresses, the van der Waals (vdW) heterostructures made of 2DLMs have attracted the interest of many researchers.[7–11] The stronger covalent bonding of the monolayer structure in heterostructure ensures its stability in the plane, while the stacked layers are linked together by vdW interactions. The different materials that comprise the heterostructures have a large degree of freedom, breaking the limitations of a single 2DLMs for applications such as electronic devices. For instance, graphene is one of the highest electronic conductivity, but without a bandgap switch, the current cannot be controlled, which greatly hinders its wide application in electronic devices.[12] The photogenerated electrons and holes of g-C_3N_4 and In_2SeS monolayers recombine easily, limiting their application in photocatalytic water splitting. The In_2SeS/g-C_3N_4 heterostructures to effectively prevent the recombination of photogenerated electrons and holes.[13] The heterostructures can combine the excellent properties of 2DLMs, resulting in superior performance over monolayer.[14,15] The excellent surface diffusions of lithium polysulfifides on C_4N_4 resulted in a fast charge/discharge rate. Furthermore, the C_4N_4/graphyne heterostructure could improve the electrical conductivity of the structure.[16]

The performance of heterostructures depends on the material itself, and searching for new materials to develop high-performance electronic devices is significant.[17] Recently, a new member of the graphdiyne family 3N-doped graphdiyne (N-GY) has been successfully synthesized in the laboratory. It has a high surface ratio, which could be assembled into a supercapacitor with an energy density of 8.66 Wh/kg, a power density of 19.3 kW/kg and a capacitance of 250 $F{\cdot}g^{-1}$.[18,19] The N-GY layer also exhibits high tensile strength can be used for tensile energy storage and fabrication of flexible devices.[20] The porous atomic structure of graphene nanosheets disperses phonons, greatly inhibiting thermal con-

*Project supported by the National Natural Science Foundation of China (Grant Nos. 62074053 and 61674053), the Natural Science Foundation of Henan Province, China (Grant No. 202300410237), the Program for Science & Technology Innovation Talents in Universities of Henan Province, China (Grant No. 18HASTIT030), and the Fund from Henan Overseas Expertise Introduction Center for Discipline Innovation (Grant No. CXJD2019005).

†Corresponding author. E-mail: xqdai@htu.cn

© 2021 Chinese Physical Society and IOP Publishing Ltd

ductivity, which makes it unusable for the preparation of thermoelectric devices. Conversely, the sp and sp^2 carbon atom types of N-GY are not homogeneous, hence the N-GY is expected to be a design object for carbon-based thermoelectric devices.[21,22] However, the electron localization is intense at the conduction band minimum (CBM) and valence band maximum (VBM) of N-GY layer, resulting in a flat band edges. The flat band and wide forbidden bands could hinder its application of N-GY layer in optoelectronic and nanoelectronic devices.

The MoS_2 is a kind of typical transition metal dichalcogenides (TMDs), which is a promising application in optoelectronic devices[23] and field effect transistors (FETs).[3,24] Due to the quantum confinement effect, bulk MoS_2 is an indirect bandgap semiconductor, while its monolayer structure is proved to be a direct bandgap semiconductor. The formation of vdW heterostructures by vertical stacking of MoS_2 layers on different materials has been extensively studied experimentally and theoretically, *e.g.* MoS_2/stanine,[25,26] Graphene/MoS_2.[27–29] In order to extend the application of N-GY layer in electronic devices, the MoS_2 and N-GY layer are chosen to build heterostructures considering the good electronic and optical properties of MoS_2 layers.

In this work, the density functional theory (DFT) calculations were performed to systematically study the electronic and optical properties of the N-GY/MoS_2 heterostructures. The external E-field and biaxial strain can effectively adjust the bandgap and band edge positions, converting the heterostructures from type-II to type-I band alignment. In addition, the heterostructure has an optical absorption range from the visible to ultraviolet (UV) with an optical absorption coefficient of 10^5 cm^{-1}. The power conversion efficiency of the heterostructure is 17.77%, which indicates the heterostructure is a promising candidate material for solar cells. Therefore, the N-GY/MoS_2 heterostructures have potential applications in multifunctional nanoelectronic devices, photovoltaic semiconductor devices and solar cells.

2. Methods

First-principles calculations were based on density generalised function theory (DFT)[30,31] with projection-enhanced wave (PAW)[32] potentials, which were implemented in the Vienna *ab initio* simulation package (VASP).[33–35] The generalized gradient approximation (GGA) to Perdew–Burke–Ernzerhof (PBE) generalisation[34] was used to treat all electronic enchange energies DFT-D3 correction[36] was used to treat vdWs interactions. A plane-wave basis set with a cut-off energy of 480 eV and a $7\times7\times1$ k-point grid in the Brillouin zone was determined with the gamma-centred Monkhorst–Pack method.[37] The DFT-PBE method usually underestimates bandgap. Therefore, the Heyd–Scuseria–Ernzerhof (HSE06) and GW_0 methods are usually used to compensate for the bandgap values and band edges.[38] In the present study, the electronic and optical properties of isolated monolayers and N-GY/MoS_2 heterostructures were calculated using the HSE06 method.[39] Using the PBE algorithm, the energy band structure basically matches except for the underestimation of the band gap, so the PBE method was used to calculate the energy band trend of the heterostructures under the effect of an applied E-field and biaxial strain to study their electronic properties. All geometries were completely relaxed until the energy and force converged to 10^5 eV and 0.01 eV/Å, respectively. To avoid interactions between adjacent layers, a vacuum layer of 20 Å was added in the Z direction.

3. Results and discussion

3.1. Geometric construction and stability

The optimized lattice constants of structurally relaxed MoS_2 and N-GY monolayers are $a=b=3.18$ Å and $a=b=11.60$ Å, respectively, which are consistent with previous theoretical and experimental results.[17,18,40] To ensure effective lattice matching, the constructed N-GY/MoS_2 heterostructures are composed of $\sqrt{13}\times\sqrt{13}$ supercell of MoS_2 and a unit cell of N-GY. The lattice mismatch is only 1.1%, which is so small that the experimental fabrication of such heterostructure would be highly achievable. As shown in Fig. 1, three typical geometric structures were considered.

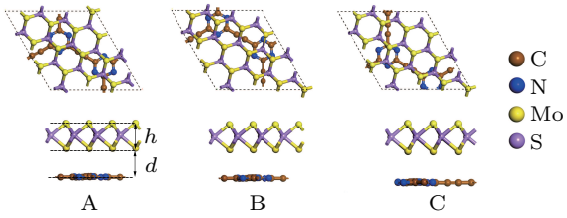


Fig. 1. The top and side views of the optimized structure N-GY/MoS_2 vdW heterostructures.

To assess the stability of the N-GY/MoS2 heterostructures, the binding energy (E_b) has been calculated using the definition

$$E_b = E_{\text{N-GY/MoS}_2} - E_{\text{MoS}_2} - E_{\text{N-GY}}, \tag{1}$$

where the $E_{N-GY/MoS2}$, E_{MoS2}, and E_{N-GY} are the total energy of the N-GY/MoS_2 heterostructures, MoS_2, and N-GY layer, respectively. For the N-GY/MoS_2 heterostructures, the layer spacing d, binding energy E_b, and thickness h of MoS_2 are listed in Table 1. By comparison, the type-C heterostructure has the lowest binding energy of -0.497 eV, implying type-C stacking is the most stable structure. In the following discussion, we only consider type-C N-GY/MoS_2 heterostructures. As shown in Fig. 1(C), the thickness h (3.105 Å–3.101 Å) of MoS_2 layer in the N-GY/MoS_2 vdW heterostructure is slightly smaller than that in intrinsic monolayer MoS_2 (3.115 Å), due to the compressive strain of MoS_2 during the formation of the heterostructures, which is similar to other vdW heterostructures.[41–43]

Table 1. Calculated interlayer spacing d, the thickness h of MoS_2, and the binding energy (E_b) of N-GY/MoS_2 vdW heterostructures.

	Type-A	Type-B	Type-C
d (Å)	3.485	3.384	3.391
h (Å)	3.103	3.105	3.101
E_b (eV)	−0.444	−0.436	−0.497

In Figs. 2(a) and 2(b), the kinetic stability of N-GY and MoS_2 monolayer are confirmed by its phonon dispersion, where no imaginary phonon branches can be found. To check the dynamic stability of the heterostructures, *ab initio* molecular dynamics (AIMD) simulations were performed using a 2×2 supercell containing 96 atoms at room temperature (300 K) for a total time of 9.6 ps with a controlled time step of 1 fs. The variation of energy and temperature with time during the simulation are shown in Fig. 2(c). The amplitude of the oscillations in the total energy is relatively small, there is no significant deformation or bond breakage in the heterostructure, thus indicating that the heterostructure has a good thermodynamic stability.

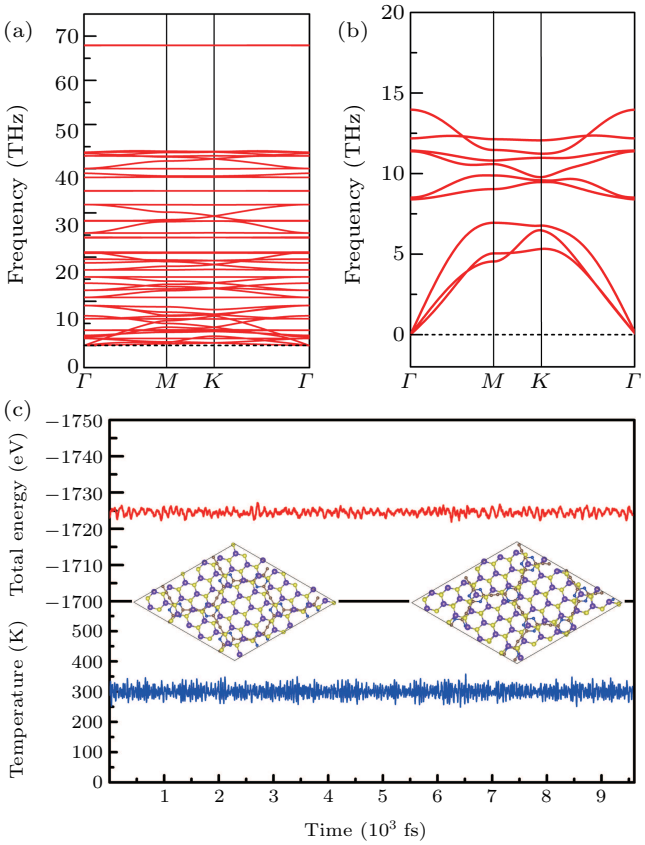


Fig. 2. Phonon band structures of the (a) N-GY, (b) MoS_2. (c) Variations of temperature and energy as a function of time for AIMD simulations of the N-GY/MoS_2 vdW heterostructure.

3.2. Electronic properties

The band structures of the N-GY and MoS_2 monolayers are shown in Figs. 3(a) and 3(b). The MoS_2 layer exhibits an indirect bandgap of 2.13 eV, while N-GY monolayer exhibits bandgap of 3.90 eV, which are agree with the experimental results.[44] As shown in Fig. 3(a), the VBM and CBM are flat in N-GY layer, and the flat band appears due to Bloch phase extinction of the electrons in six-membered ring formed by the C and N atoms, where the electrons are tightly localized. The flat band is the opposite extreme to the Dirac band, where the intersection of conduction and valence bands exhibit a complete linear dispersion relationship, with massless and very fast electrons. In the flat band, the dispersion is zero, the kinetic energy of the electron is quenched, the effective mass is infinite and the density of states is very large.[41,45–49]

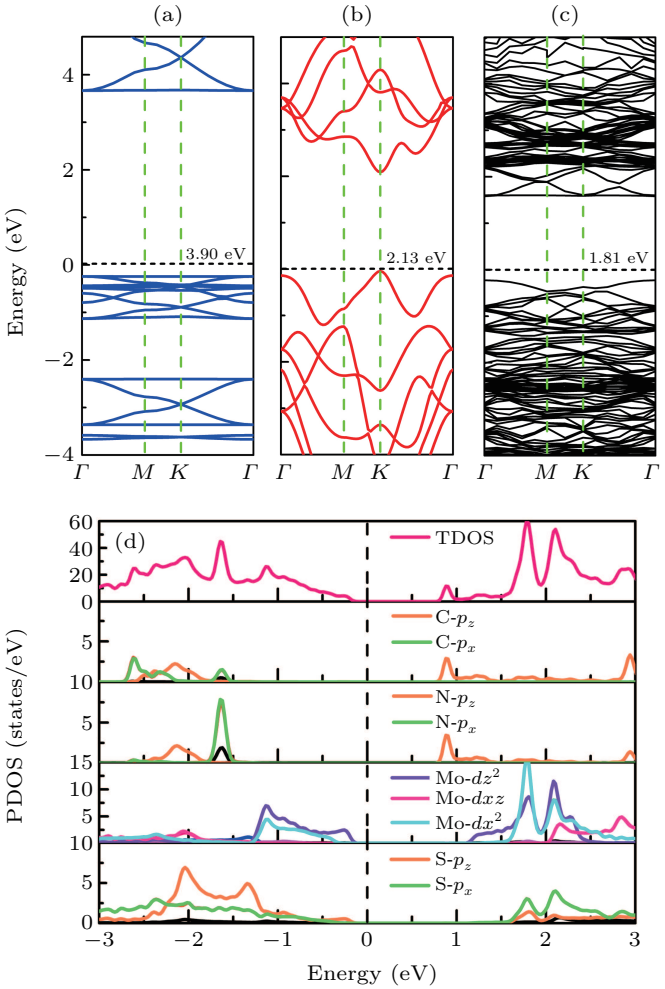


Fig. 3. The band structures of (a) N-GY, (b) MoS_2, and (c) N-GY/MoS_2 heterostructures. (d) The total and projected density states of N-GY/MoS_2 heterostructures.

The electronic properties of the N-GY/MoS_2 heterostructure are presented in Fig. 3(c). The bandgap of the N-GY/MoS_2 heterostructure is 1.81 eV. The projected density of states (PDOS) of the N-GY/MoS_2 heterostructure is shown in Fig. 3(d). From the PDOS, it can be observed that the CBM and VBM of the N-GY/MoS_2 heterostructures are contributed by N-GY layer and MoS_2 layer, respectively, which exhibits a typical type-II band alignment. The CBM is mainly contributed by the p_z orbital electrons of the C and N atoms of the N-GY layer, which is the main source of the flat band. The VBM is contributed by the d_{z^2} orbital of the Mo atoms of the MoS_2 layer.

When different materials form a heterostructure, the difference in the work function causes a directional movement of electrons between the two layers.[16,25,50] The planar average electrostatic potentials along the Z direction for N-GY, MoS_2 layer, and N-GY/MoS_2 heterostructures are shown in Fig. 4. The work functions (Φ) of the N-GY and MoS_2 layer are 6.93 eV and 5.67 eV, respectively, which are consistent with previous reports.[2] The work function of the heterostructure is 5.52 eV, which are lower than that of the intrinsic monolayer N-GY and MoS_2, respectively 1.41 eV and 0.15 eV smaller.

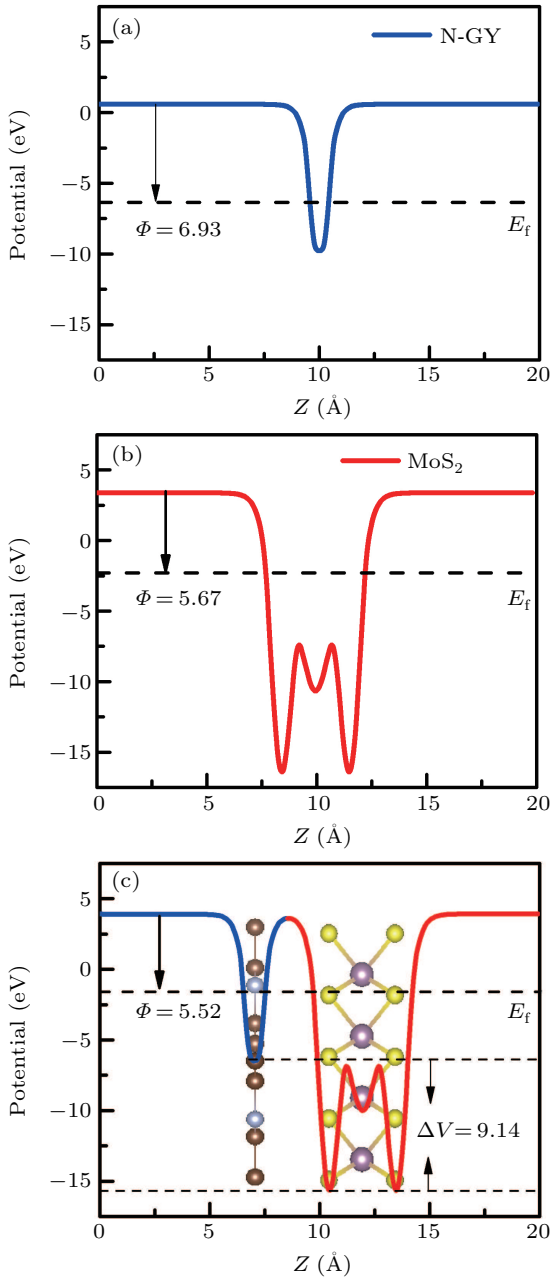


Fig. 4. The average electrostatic potential for the N-GY monolayer (a), MoS_2 monolayer (b), and N-GY/MoS_2 heterostructures (c), respectively.

Due to the difference of work functions between N-GY layer and MoS_2 layer, the electrons spontaneously transfer from MoS_2 layer to N-GY layer until their Fermi levels are aligned. In the interface region, positive charges accumulate in MoS_2 layer and negative charges accumulate in N-GY layer, forming a built-in E-field (E_{int}), whose direction is directed from MoS_2 to N-GY layer. There is a potential drop of 9.14 eV in the N-GY/MoS_2 heterostructure. The potential drop can easily drive electrons from MoS_2 to N-GY, thus the concentration of holes in MoS_2 and the electron carrier concentration in N-GY can be amplified.

To better investigate the charge transfer mechanism at interfaces of heterostructures, in Fig. 5 we calculate the plane-averaged charge density difference (CDD), the CDD can be obtained by the following formula:

$$\Delta\rho = \int \rho_{\text{N-GY/MoS}_2}(x,y,z)\,\mathrm{d}x\mathrm{d}y - \int \rho_{\text{N-GY}}(x,y,z)\,\mathrm{d}x\mathrm{d}y - \int \rho_{\text{MoS}_2}(x,y,z)\,\mathrm{d}x\mathrm{d}y, \quad (2)$$

in the above equation, $\rho_{\text{N-GY/MoSe}_2}(x,y,z)$, $\rho_{\text{N-GY}}(x,y,z)$, and $\rho_{\text{MoS}_2}(x,y,z)$ are the charge densities of N-GY/MoS_2 heterostructures, MoS_2, and N-GY layers, respectively. From Eq. (2), a positive value is defined as an accumulation of charge and a negative value represents the depletion of electric charges. As seen in Fig. 5, the charges are redistributed at the interface of heterostructures, depleted in the N-GY layer (red) and accumulated at the S-atom position in the MoS_2 layer (cyan). The electron transfer number from MoS_2 layer to N-GY layer is 0.465e by Bader charge analysis. The charge rearrangement phenomenon generally leads to the formation of electron–hole depressions at the N-GY/MoS_2 heterostructures interface.[44]

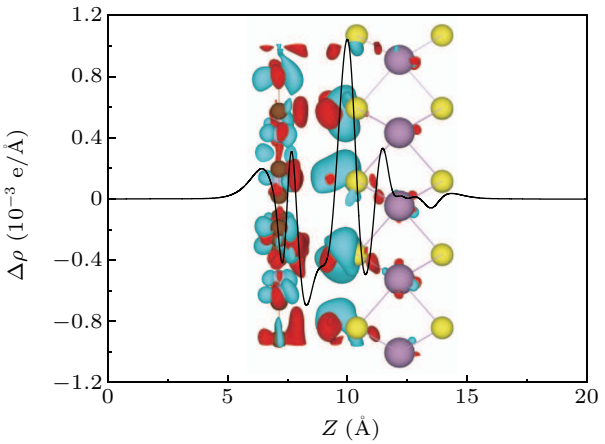


Fig. 5. The inset is the 3D isosurfaces of the charge density difference, the cyan and red areas represent charge accumulation and depletion, respectively, and the isosurfaces value is 0.0005 e/Å^3.

3.3. Electric field effects on N-GY/MoS_2 heterostructures

The adjustability of electronic structure is significant for the application of materials in electronic devices, and the external electric field (E-field) is an effective method for regulating the band alignment.[51] Figure 6(a) shows the relationship between the bandgap of N-GY/MoS_2 heterostructures and

external E-field. Here, we consider two external E-field directions ($+z$, $-z$) perpendicular to the plane of heterostructure atoms. The positive direction is that the N-GY layer points to the MoS_2 layer, and the range is from -1.0 V/Å to 1.0 V/Å. When the $+z$ E-field is applied, the bandgap of the heterostructures first increases and then remains unchanged, with the increase of the E-field strength, reaching the maximum value of 1.39 eV at the E-field = 0.2 V/Å. The bandgap remains basically constant at the E-field of 0.2 V/Å–0.8 V/Å, because the direction of the external E-field is opposite to the $E_{\rm int}$ direction in the heterostructures. The bandgap gradually decreases with the E-field strength further increasing. Conversely, when an external $-z$ E-field in the same direction as $E_{\rm int}$ is applied, the total E-field is enhanced. The bandgap decreases further sharply with the external E-field increase from 0 V/Å to -0.7 V/Å. Its bandgap could be zero at E-field > -0.7 V/Å, which suggests that the heterostructure could be tuned from semiconductor to metallic properties.

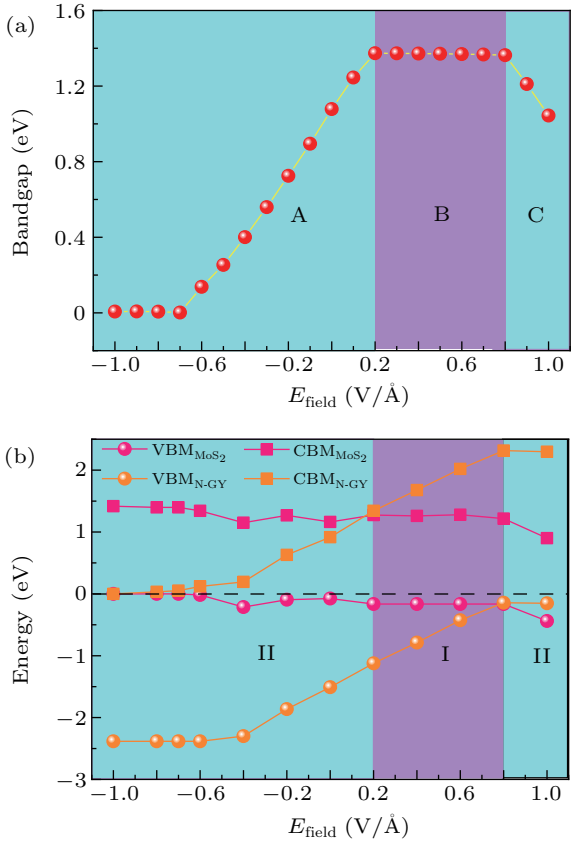


Fig. 6. The evolution of the bandgap (a) and the band edges (b) of the N-GY/MoS_2 heterostructures as a function of E-field.

The variation of band edges of N-GY/MoS_2 heterostructures under different external E-fields are presented in Fig. 6(b). The CBM and VBM of MoS_2 in the heterostructures continue to move down with the increase of the positive E-field strength, while the CBM and VBM of N-GY layer continue to rise. When the external E-field = 0.2 V/Å, the CBM of MoS_2 layer is lower than that of N-GY. Both the CBM and VBM of the heterostructures are contributed by the MoS_2 layer, and the system transforms into a type I band alignment. Notably, when the external E-field > 0.8 V/Å, the VBM of heterostructure is contributed by N-GY and the CBM is contributed by MoS_2 layer. At this time, the system is transformed into type-II band alignment again. With an increasing reverse E-field is applied to the heterostructure, the CBM and VBM of N-GY layer in the heterostructures continue to move down, while the CBM and VBM of MoS_2 continue to rise. At the E-field = -0.7 V/Å the CBM and VBM intersect, the bandgap is closed, thus the heterostructure could change from semiconductor to metal. The predicted results of this bandgap adjustment show that the electronic properties of the heterostructures can be effectively and dynamically controlled by the external E-field, realizing the transition from type-II to type-I band alignment and from the semiconductor to metal.

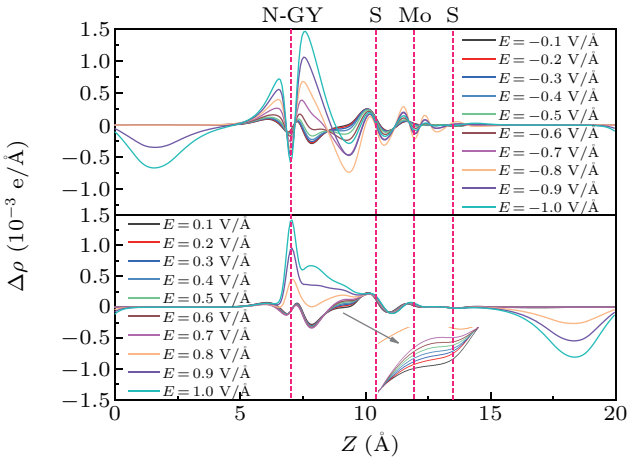


Fig. 7. The integrated charge density difference of the N-GY/MoS_2 heterostructures along the Z direction.

Furthermore, when an external E-field is applied, the charge inside the heterostructure could be redistributed. The integrated charge density difference along the Z direction was calculated as

$$\Delta\rho_{E_{\rm field}} = \int \rho^{E_{\rm field}\neq 0}_{\text{N-GY/MoS}_2}(x,y,z)\,{\rm d}x{\rm d}y - \int \rho^{E_{\rm field}=0}_{\text{N-GY/MoS}_2}(x,y,z)\,{\rm d}x{\rm d}y, \tag{3}$$

where

$$\int \rho^{E_{\rm field}\neq 0}_{\text{N-GY/MoS}_2}(x,y,z)\,{\rm d}x{\rm d}y,$$

$$\int \rho^{E_{\rm field}=0}_{\text{N-GY/MoS}_2}(x,y,z)\,{\rm d}x{\rm d}y$$

denote the charge density at the point in the Z direction for the heterostructures with and without an external E-field, respectively. From the formula, a negative value indicates a depletion of charge and a positive value indicates an accumulation of charge. Figure 7 shows the planar average charge density along the Z direction for N-GY/MoS_2 heterostructures. The amount of charge transfer is proportional to the strength of the external E-field and independent of the direction of external E-field. Notably, a certain charge density also

appears in the vacuum layer at larger E-field strengths due to dielectric breakdown and charge tunneling, which is similarly observed for the arsenic/C_3N, blue phosphorus/C_2N, and Sb/InSe heterostructures.[52–54]

3.4. Strain effects on N-GY/MoS_2 heterostructures

Biaxial strain is one of the effective ways in which the electronic structure of layered materials can be tuned. Figure 8(a) illustrates the bandgap as a function of biaxial strain ($\varepsilon = -4\%$ to 4%). The biaxial strain is defined as $\varepsilon = \Delta l/l \times 100\%$, where Δl and l denote the change in lattice constant and the intrinsic lattice constant, respectively. When tensile strain is applied to the system, the bandgap of the heterostructures monotonically decreases. With compressive strains are applied, the bandgap of the heterostructure increases and then decreases, reaching a maximum of 1.19 eV at $\varepsilon = -2\%$. The variations of the band alignment of the N-GY/MoS_2 heterostructures with strains are presented in Fig. 8(b). From 0% to -4% of strains, the CBM of MoS_2 shifts upwards with increasing strains, but is always higher than the CBM of N-GY layer. At this point, the VBM of heterostructure is contributed by MoS_2, the CBM is contributed by N-GY, and the system shows a type-II band alignment. When tensile strain is applied, the CBM of MoS_2 moves down with the increase of strain. At the $\varepsilon = 2\%$, both VBM and CBM of the heterostructures are contributed by MoS_2, and the system is transformed into type-I band alignment. The above results show that biaxial strain can effectively regulate the band structure of heterostructures to achieve the transition from type-II to type-I band alignment.

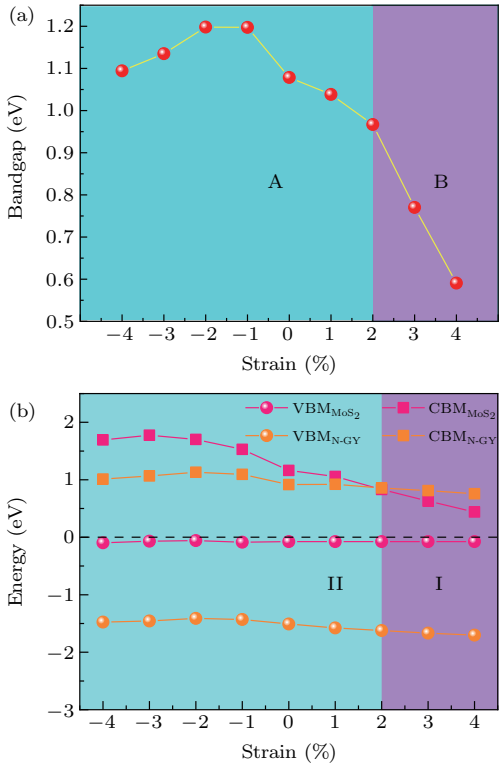


Fig. 8. The evolution of the bandgap (a) and the band edges (b) of N-GY/MoS_2 heterostructure as a function of strain.

3.5. Optical properties

The optical absorption coefficients of the N-GY/MoS_2 heterostructures are presented in Fig. 9. The optical absorption coefficient is defined by the following equation:

$$\alpha(\omega) = \sqrt{2}\frac{\omega}{c}\left[\sqrt{\varepsilon_1^2(\omega)+\varepsilon_2^2(\omega)} - \varepsilon_1(\omega)\right]^{1/2}, \quad (4)$$

where $\varepsilon_1(\omega)$ and $\varepsilon_2(\omega)$ are the real and imaginary parts of the complex dielectric function, respectively. The first absorption peak of the intrinsic N-GY layer is in the UV region and the absorption coefficient is almost zero in the visible range. The N-GY/MoS_2 heterostructures can break through the restrictions of isolating layer and combine their optical absorption strength together. The N-GY/MoS_2 heterostructure is found to absorb a wide range of solar spectrum in the visible region as compared to the constituent monolayers. In the UV-visible light the optical absorption coefficient is 10^5 cm^{-1}, the type-II band alignment facilitates exciton–hole complexation and increases exciton lifetime. Good absorbance is essential for its performance in optoelectronic and photovoltaic applications. By comparing the band edges of monolayers forming type-II band alignment, the application prospect of this heterostructure in 2D exciton solar cell is prospected.

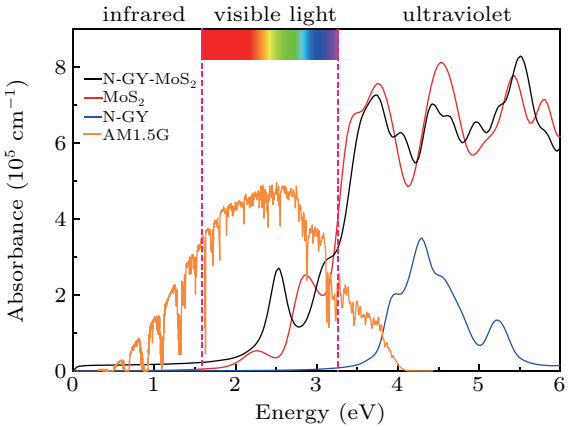


Fig. 9. Optical absorption coefficients of MoS_2, N-GY, and N-GY/MoS_2, heterostructures at the HSE06 level.

The power conversion efficiency (PCE) of N-GY/MoS_2 heterostructures can be evaluated as[55]

$$\eta = \frac{J_{sc}V_{oc}\beta_{FF}}{P_{solar}} = \frac{0.65(E_g - \Delta E_c - 0.3)\int_{E_g}^{\infty}\frac{P(\hbar\omega)EQE(\hbar\omega)}{\hbar\omega}\mathrm{d}(\hbar\omega)}{\int_0^{\infty}P(\hbar\omega)\mathrm{d}(\hbar\omega)}, \quad (5)$$

where 0.65 is the band-fill factor (β_{FF}), E_g is the bandgap of the donor, and the term $(E_g - \Delta E_c - 0.3)$ evaluates the maximum open-circuit voltage V_{oc}. The $P(\hbar\omega)$ is the air mass 1.5 (AM1.5) solar energy flux at the photon energy $\hbar\omega$. $EQE(\hbar\omega)$ is the external quantum efficiency and is assumed to 100%. The integral in the numerator depicts the short-circuit current J_{sc} in the limit of 100% $EQE(\hbar\omega)$ while the denominator is

the solar energy flux at AM1.5. The calculated PCE for the intrinsic N-GY/MoS_2 heterostructures is 17.77%, which is comparable to the recently reported, such as phosphorene/MoS_2 (18%–21%)[56] and GeSe/SnS heterobilayers (∼ 18%).[57] As shown in Fig. 10(b), we design the N-GY/MoS_2 heterostructures as a solar cell with Au and ITO as electrode material, N-GY layer as the acceptor and the MoS_2 layer as the donor, respectively.

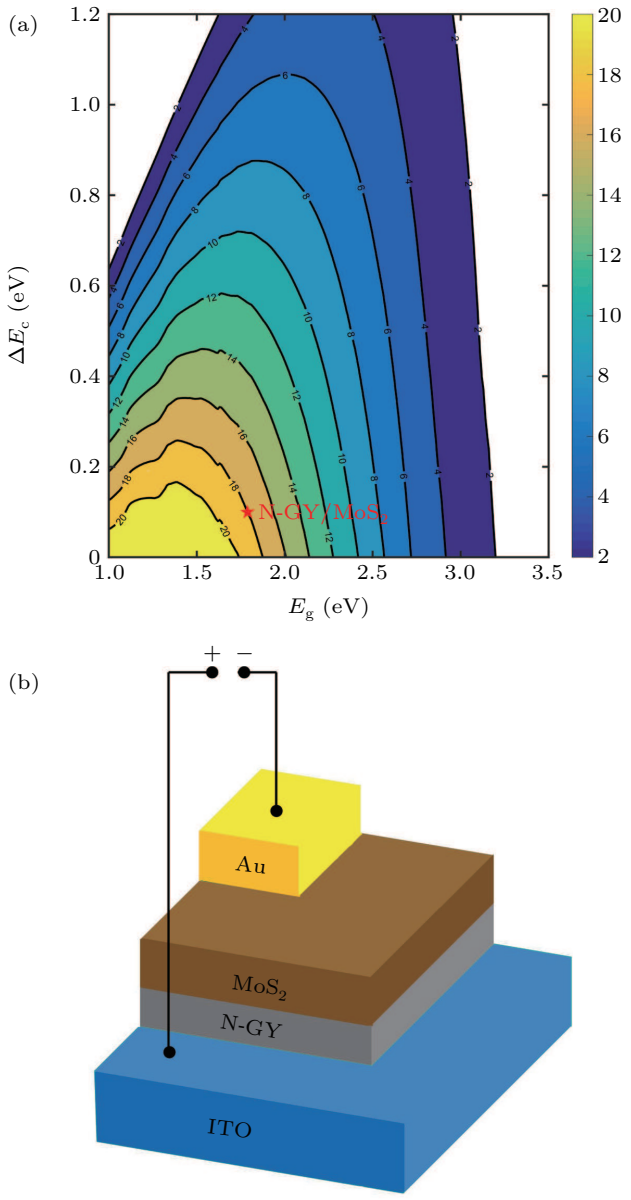


Fig. 10. (a) The power conversion efficiency of N-GY/MoS_2 heterostructures. (b) Schematic illustration of the thin-film solar cell.

4. Conclusion

In summary, density functional theory calculations were performed to systematically study the electronic and optical properties of the N-GY/MoS_2 heterostructures. The binding energy and molecular dynamics simulations demonstrate that N-GY/MoS_2 van der Waals heterostructures could exist stably. The external E-field and biaxial strain can effectively adjust the bandgap and band edge positions, converting the heterostructures from type-II to type-I band alignment. The bandgap of the heterostructures varies in trend under different external E-fields, varying linearly in the range of −0.7 V/Å to 0.2 V/Å and 0.8 V/Å to 1.0 V/Å, but remaining essentially constant in the range of 0.2 V/Å to 0.8 V/Å. The charge transfer is proportional to the strength of external E-field. In addition, the heterostructure exhibits an excellent optical absorption coefficient of 10^5 cm^{-1}, range from visible to UV. The power conversion efficiency of N-GY/MoS_2 heterostructure is high to 17.77%, suggesting this heterostructure is a promising candidate for solar cells. Our work shows that N-GY/MoS_2 heterostructure is a candidate material for semiconductor sensors and photovoltaic devices due to effective charge separation, tuned band alignment, broad optical absorption spectrum, high optical absorption intensity, and high power conversion efficiency.

Acknowledgment

The authors thank the high performance computing center of Henan Normal University.

References

[1] Novoselov K S, Geim A K, Morozov S V, Jiang D, Zhang Y, Dubonos S V, Grigorieva I V and Firsov A A 2004 *Science* **306** 666
[2] Tongay S, Zhou J, Ataca C, Lo K, Matthews T S, Li J B, Grossman J C and Wu J Q 2015 *Nano Lett.* **12** 5576
[3] Mak K F, Lee C, Hone J, Shan J and Heinz T F 2010 *Phys. Rev. Lett.* **105** 136805
[4] Ahin H, Cahangirov S, Topsakal M, Bekaroglu E and Ciraci S 2009 *Phys. Rev. B* **80** 155453
[5] Cahangirov S, Topsakal M, Aktuerk E, Sahin H and Ciraci S 2009 *Phys. Rev. Lett.* **102** 236804
[6] Li T T, He C and Zhang W X 2020 *Energy Storage Materials* **25** 866
[7] Novoselov K S, Mishchenko A, Carvalho A and Neto A C 2016 *Science* **353** 9439
[8] Buscema M, Island J O, Groenendijk D J, Blanter S I and Steele G A 2015 *Chem. Soc. Rev.* **44** 3691
[9] Fang H, Battaglia C, Carraro C, Nemsak S, Ozdol B, Kang J S, Bechtel H A, Desai S B, Kronast F and Unal A A 2014 *Proc. Natl. Acad. Sci. USA* **111** 6198
[10] Li T T, He C and Zhang W X 2021 *J. Energy Chem.* **52** 121
[11] He C, Liang Y and Zhang W X 2021 *Appl. Surf. Sci.* **553** 149550
[12] Zhang W X, Yin Y and He C 2020 *Phys. Chem. Chem. Phys.* **22** 26231
[13] He C, Han F S, Zhang J H and Wang W X 2020 *J. Mater. Chem. C* **8** 6923
[14] Ceballos F, Bellus M Z, Chiu H Y and Zhao H 2014 *ACS Nano* **8** 12717
[15] Padilha J E, Fazzio A and Silva A J R D 2015 *Phys. Rev. Lett.* **114** 66803
[16] Li T T, He C and Zhang W X 2019 *J. Mater. Chem. A* **7** 4134
[17] Zhao N and Schwingenschlgl U 2020 *Nanoscale* **12** 11448
[18] Mortazavi B, Shahrokhi M, Madjet E A, Hussain T, Zhuang X and Rabczuk T 2019 *J. Mater. Chem. C.* **7** 3025
[19] Shang H, Zuo Z, Zheng H, Li K, Tu Z, Yi Y, Liu H, Li Y and Li Y 2018 *Nano Energy* **44** 144
[20] Pan Q Y, Liu H, Zhao Y J, Chen S Q, Xue B, Kan X N, Huang X W, Liu J and Li Z B 2018 *ACS Appl. Mater. Inter.* **11** 2740
[21] Sun L, Jiang P H, Liu H J, Fan D D, Liang J H, Wei J, Cheng L, Zhang J and Shi J 2015 *Carbon* **90** 255
[22] Wang X and Lu S 2013 *J. Phys. Chem. C* **117** 19740
[23] Lloyd D, Liu X, Christopher J W, Cantley L, Wadehra A, Kim B L, Goldberg B B, Swan A K and Bunch J S 2016 *Nano Lett.* **16** 5836
[24] Mak K F, He K, Shan J and Heinz T F 2012 *Nat. Nanotechnol.* **7** 494
[25] Xiong W, Xia C, Du J, Wang T, Peng Y, Wei Z and Li J 2017 *Nanotechnology* **28** 195702

[26] Ren C, Feng Y, Zhang S, Zhang C and Wang P 2017 *RSC Adv.* **7** 9176
[27] Loan P T K, Zhang W, Lin C, Wei K, Li L and Chen C 2014 *Adv. Mater.* **26** 4838
[28] Yu W J, Li Z, Zhou H, Chen Y, Wang Y, Huang Y and Duan X 2013 *Nat. Mater.* **12** 246
[29] Choi M S, Lee G H, Yu Y J, Lee D Y, Lee S H, Kim P, Hone J and Yoo W J 2013 *Nat. Commun.* **4** 1624
[30] Kohn W and Sham L J 1965 *Phys. Rev. A* **140** A1133
[31] Nityananda R, Hohenberg P and Kohn W 2017 *Resonance* **22** 809
[32] Kresse G and Furthmüller J 1996 *Comp. Mater. Sci.* **6** 15
[33] Kresse G and Joubert D 1999 *Phys. Rev. B* **59** 1758
[34] Perdew J P, Burke K and Ernzerhof M 1998 *Phys. Rev. Lett.* **77** 3865
[35] Kresse G and Furthmüller J 1996 *Phys. Rev. B* **54** 11169
[36] Grimme S, Antony J, Ehrlich S and Krieg H 2010 *J. Chem. Phys.* **132** 154104
[37] Monkhorst H J and Pack J D 1976 *Phys. Rev. B* **13** 5188
[38] Xia C X, Du J, Huang X W, Xiao W B and Xiong W Q 2018 *Phys. Rev. B* **97** 115416
[39] Xia C X, Du J, Xiong W Q, Jia Y, Wei Z M and Li J B 2017 *J. Mater. Chem. A* **5** 13400
[40] Lu N, Guo H Y, Li L, Dai J, Wang L, Mei W N, Wu X J and Zeng X C 2014 *Nanoscale* **6** 2879
[41] Wei H, Li Z, and Yang J 2013 *J. Chem. Phys.* **138** 124706
[42] Du A J, Sanvito S, Li Z, Wang D W, Jiao Y, Liao T, Sun Q, Ng Y H, Zhu Z H and Amal R 2012 *J. Am. Chem. Soc.* **134** 4393
[43] Giovannetti G, Khomyakov P A, Brocks G, Kelly P J and Brink J 2007 *Phys. Rev. B* **76** 073103
[44] Pan H, Zhang H, Wang H, Li J and Wang X 2020 *Appl. Surf. Sci.* **513** 145694
[45] Pan H Z, Yin H, Li J F, Zhang H Y, Du Y W and Tang N J 2018 *Phys. Chem. Chem. Phys.* **20** 14166
[46] Mina M, Nguyen T C and Susumu O 2016 *Carbon* **109** 755
[47] Zhong C, Xie Y, Chen Y and Zhang S 2016 *Carbon* **99** 65
[48] Endo S, Oka T and Aoki H 2010 *Phys. Rev. B* **81** 113104
[49] Miao Z, Zheng L, Ming W, Wang Z and Feng L 2014 *Phys. Rev. Lett.* **113** 236802
[50] Xiong W Q, Xia C X, Zhao X, Wang T X and Jia Y 2016 *Carbon* **109** 737
[51] Ma Y Q, Zhao X, Wang T X, Li W, Chang S S, Wang X, Li Y, Zhao M Y and Dai X Q 2016 *Phys. Chem. Chem. Phys.* **18** 28466
[52] Zhang Z, Xie Z, Liu J, Tian Y, Zhang Y, Wei X, Guo T, Ni L, Fan J and Weng Y 2020 *Phys. Chem. Chem. Phys.* **22** 5873
[53] Zhang Z H, Zhang Y, Xie Z, Wei X, Guo T T and Fan J B 2019 *Phys. Chem. Chem. Phys.* **21** 5627
[54] Zeng H, Zhao J, Cheng A Q, Zhang L, He Z and Chen R S 2017 *Nanotechnology* **29** 075201
[55] Fan Y C, Wang J R and Zhao M W 2019 *Nanoscale* **11** 14836
[56] Kaur S, Kumar A, Srivastava S, Tankeshwar K and Pandey R 2018 *J. Phys. Chem. C* **122** 26032
[57] Mao Y L, Xu C S, Yuan J M and Zhao H 2019 *J. Mater. Chem. A* **7** 11265